Diffusion and directed motion in cellular transport

Avi Caspi, Rony Granek, and Michael Elbaum
Department of Materials and Interfaces, Weizmann Institute of Science, Rehovot 76100, Israel
(Received 11 October 2001; published 29 July 2002)

We study the motion of a probe driven by microtubule-associated motors within a living eukaryotic cell. The measured mean square displacement, $\langle x(t)^2\rangle$ of engulfed 2 and 3μm diameter microspheres shows enhanced diffusion scaling as $t^{3/2}$ at short times, with a clear crossover to ordinary or subdiffusive scaling, i.e., t^{γ} with γ less than or equal to 1, at long times. Using optical tweezers we tried to move the engulfed bead within the cell in order to relate the anomalous diffusion scaling to the density of the network in which the bead is embedded. Results show that the larger beads, 2 and 3μm diameter, must actively push the cytoskeleton filaments out of the way in order to move, whereas smaller beads of 1μm diameter can be ''rattled'' within a cage. The 1 μm beads also perform an enhanced diffusion but with a smaller and less consistent exponent $1.2<\gamma<1.45$. We interpret the half-integer power observed with large beads based on two diverse phenomena widely studied in purified cytoskeleton filaments: (1) the motion of the intracellular probe results from random forces generated by motor proteins rather than thermal collisions for classical Brownian particles, and (2) thermal bending modes of these semiflexible polymers lead to anomalous subdiffusion of particles embedded in purified gel networks or attached to single filaments, with $\langle x(t)^2\rangle \sim t^{3/4}$. In the case of small beads, there may also be a Brownian contribution to the motion that results in a smaller exponent.

DOI: 10.1103/PhysRevE.66.011916 PACS number(s): 87.17.−d, 87.16.Ka

I. INTRODUCTION

The eukaryotic cell generates directed forces in order to distribute components among internal compartments, to import and export materials, and to apply forces to external objects. We have shown that in certain cellular models, a particle adhering to the cell surface near its periphery becomes engulfed into the cell and performs a directed centripetal motion. The directionality of this motion ends near the nuclear region, where it continues to move randomly within a restricted space [1]. The random ''wandering'' near the nucleus appears to be similar to diffusive motion, but displays a mean square displacement (MSD) $\langle x(t)^2\rangle$ proportional to t^{γ}, with $\gamma=3/2$ rather than $\gamma=1$ for Brownian motion. Values of $\gamma>1$ are classified as enhanced diffusion [2] and inside the cell this phenomenon is caused by a collective activity of protein motors rather than thermal kicks [3]. Those motors are used to move cargos back and forth along the microtubules between different regions and compartments within the cell.

Enhanced diffusion with 3/2 scaling was previously discussed theoretically in the context of a random velocity field [4,5]. Recently, enhanced diffusion was observed in the swimming activity of bacteria, and interpreted as a crossover between ballistic and diffusion time regimes [6]. We argued [3] that in our case, i.e., within the living cell, the anomalous $t^{3/2}$ scaling is due to microtubule-associated motor proteins giving rise to the driven motion while the surrounding microtubule network (Fig. 1) inhibits this motion by introducing a time-dependent drag. Therefore the $t^{3/2}$ scaling effectively represents an inhibited ballistic regime, rather than enhancement of a thermal diffusion process. In this paper, the effect of intimate contact between the cytoskeletal network and the bead will be studied by using beads with various sizes relative to the effective mesh size of the network. The particle dynamics will be evaluated by measuring the MSD, while the space available for the bead to diffuse will be measured by ''rattling'' it within the cell using optical tweezers.

The paper will consist of the following sections. First, a brief description of the cytoskeletal filaments, i.e., actin and microtubules, will be presented. Then the thermal undulation of these semiflexible polymers will be discussed at the level of individual filaments, with particular attention to the anomalous scaling of the mean square displacement of a point along the polymer. Following, we will summarize and integrate previous experiments in which scaling laws were measured directly in a purified network of microtubules [7]. Those results are used to explain measurements of enhanced

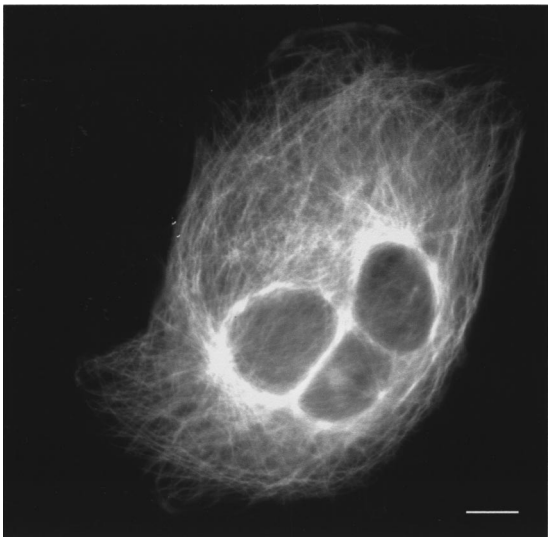

FIG. 1. Immunofluorescence image of the microtubule network of a giant multinuclear SV80 fibroblast. Cells were fixed in cold methanol, then stained by a primary antibody for α tubulin and a secondary fluorescently labeled antibody. Scale bar 10 μm.

diffusion of an intracellular probe [3]. Next, the mean square displacement is measured on beads of various sizes, and we relate the observed scaling to the space available for the bead to move. Measurements were made using video particle tracking as well as using a method based on continuous-wave two-photon fluorescence excitation by the optical tweezers.

II. SEMIFLEXIBLE BIOPOLYMERS

Filaments of the cytoskeleton have recently drawn attention as a subject for experiments and theories with many interesting physical implications. The major cytoskeleton networks are made of filamentous actin (F-actin) and microtubules (MT). These build distinct but interconnected intracellular networks. F-actin is most closely associated with maintenance of cell shape and generation of contractile forces, while microtubules are primarily responsible for the internal cell structure and organization. In addition to their function in supporting the cell structure and providing mechanical rigidity, those filaments play a major role in generating directed forces. They form tracks on which specific enzymes, commonly called ''motor proteins,'' move by converting chemical energy derived from adenosine triphosphate (ATP) hydrolysis into mechanical work.

Actin filaments are double-stranded helical polymers of the monomeric globular protein, with a diameter of roughly 7 nm. Various types of the motor protein *myosin* use the chemical energy derived from ATP hydrolysis to move along actin filaments. The actin-myosin motory system drives the sliding of adjacent actin filaments against each other, resulting in dynamic construction of organized stress fibers, muscle contraction, and cell movements. Various types of unconventional myosins can move directionally along single actin filaments.

Microtubules, the focus of our experiments, are long hollow cylinders made of the protein tubulin, with an outer diameter of 25 nm. They are much more rigid than actin filaments. The MT are built from 13 linear protofilaments, each composed of alternating α- and β-tubulin subunits, bound in parallel to form a cylinder. Since the 13 protofilaments are aligned in parallel with the same polarity, the microtubule itself is a polar structure, defining so-called plus and minus ends. Each subunit is oriented in such a manner that the α tubulin points toward the minus end while the β tubulin points toward the plus end [8].

Microtubule polymerization and depolymerization are dynamic processes and have important biological, chemical, and physical roles. Purified tubulin, above a critical concentration [9], will polymerize into MT near room temperature *in vitro*. The plus end of the MT can be seen to elongate at approximately three times the rate of the minus end [10,11]. In the cell, they nucleate from the microtubule-organizing center, or the centrosome, so as to form radial tracks that establish inward and outward directionality. Two classes of MT-dependent motor proteins were identified and isolated, the *kinesins* and *dyneins*. Each motor protein moves in only one direction along a MT. Most kinesin types move toward the plus end (the cell periphery), whereas dyneins move toward the minus end (the interior of the cell). *In vitro* experiments have measured a stall force of a few piconewtons for the microtubule-kinesin motor interaction [12]. A similar stall force was measured in the case of an actin-myosin interaction [13]. It was also shown, for microtubules, that the generated force has a duration of a few seconds [14,15].

The biological role and exceptional elastic properties of the cytoskeletal filaments have motivated *in vitro* physical experiments. The stiffness of a filament defines a persistence length, the scale on which thermal undulations decorrelate the tangent vectors of distant segments along the filament. The persistence length (L_P) is equal to the ratio of the bending rigidity (κ) of the filament to the thermal energy ($L_P \sim \kappa/k_BT$) [16–18]. The high stiffness of F-actin and microtubules expands the space and time scales for diffusive and undulatory movements relative to conventional polymers, thus enabling elasticity measurements at the level of a single filament or a network using optical microscopy techniques.

Analysis of microtubules' fluctuations in shape has been used to extract their persistence length. Fluctuations were generated by thermal energy [19], hydrodynamic flow [20], or by optical tweezers [21]. Alternately, microtubule bending rigidity was measured by enclosing the filament into a vesicle, and viewing its buckling while increasing the tension in the membrane by micropipet aspiration [22]. Shape analysis was used for actin filaments in order to measure their persistence length. Experiments based on thermal fluctuation of actin filaments were interpreted by a variety of techniques: comparing the mean square end-to-end distance to the filament contour length [23], extracting the correlation function given by the mean vector inner product between unit tangent vectors along the filament [24], and measuring the amplitude variance of each Fourier mode [19]. Shape analysis of the actin filament was also performed in the presence of an external oscillatory force at one end generated by optical tweezers via an attached bead [25]. All of the above flexural rigidity measurements yield persistence lengths of 2–10 mm for microtubules, and 5–20 μm for actin filaments.

III. ANOMALOUS DIFFUSION OF SEMIFLEXIBLE POLYMERS

A point (chemical monomer) along a filament is exposed to thermal collisions from the solvent. However, it cannot diffuse freely because its motion is restricted by the neighboring monomers. Thus, diffusional dynamics of the point are governed by continuum elastic bending modes of the filaments. Equipartition of thermal energy excites all possible bending modes with amplitude inversely proportional to the bending rigidity and the square curvature. Due to the viscous interaction with the solvent, each mode has a different characteristic decay time according to its wave number. The MSD of a point at distance x along the baseline of the filament, defined by

$$\langle \Delta h^2(x,t) \rangle = \langle [h(x,t) - h(x,0)]^2 \rangle, \tag{1}$$

is a measure of the undulation amplitude $h(x,t)$ at this point.

It is given by the sum over bending modes from $n=1$ to $n=L/a$ (n is the mode number and a is the filament diameter),

$$\langle \Delta h^2(x,t)\rangle = \frac{4}{L}\sum_{n=1}^{L/a} \frac{k_B T}{\kappa q^4}(1-e^{-w(q)t})\sin^2(qx), \qquad (2)$$

where $q=n\pi/L$ is the wave number of each excited mode and $k_B T/\kappa q^4$ is its contribution to the MSD resulting from the bending energy. The relaxation rate $w(q)$ of mode q, to leading order in qa, is given by

$$w(q)\approx \frac{\kappa q^4}{4\pi\eta}\ln(1/qa), \qquad (3)$$

where η is the solvent viscosity. The amplitude of undulations comes to saturation at times longer than a characteristic time τ_S, which is the inverse of the longest mode ($q=\pi/L$) relaxation rate

$$\tau_S = w^{-1}(\pi/L) = \frac{4}{\pi^3}\frac{\eta L^4}{\kappa \ln(L/\pi a)}. \qquad (4)$$

At short times the transverse MSD of a point along the filament reduces to [26,27]

$$\langle \Delta h^2(x,t)\rangle \propto \frac{k_B T}{\eta^{3/4}\kappa^{1/4}} t^{3/4} \qquad (5)$$

with an anomalous scaling exponent of 3/4. Note that the prefactor depends on κ (i.e., L_P) and is effectively independent of L. At short times the number of contributing modes grows with time, from the shortest toward longer wavelengths. Thus, the response of the filament is more local the shorter the time span on which it is observed. Alternately, in the short time regime the monomer does not feel the finite length of the polymer. Each time interval accesses a subset of available spatial modes, q. Each mode is damped at a different time scale according to Eq. (3). The superposition of all modes, [Eq. (2)] results in the anomalous scaling law.

We were able to measure directly the 3/4 scaling law of a point on a microtubule using video microscopy [7]. Using a microsphere (bead) as a marker, we tracked optically a single point on the filament. Tubulin protein was purified from bovine brain as described in the literature [28]. A solution of cold depolymerized tubulin at 35 μM concentration was injected into the observation chamber, which consisted of a long cover slip fixed crosswise to an ordinary glass microscope slide using parafilm spacers. The microtubules polymerized at room temperature inside the sample cell. Tracking of a single point on a microtubule was enabled by chemically attaching a microsphere (bead) to a single point on a microtubule. After the network of microtubules developed, 0.3 μm diameter silica microspheres, activated so as to adhere to the microtubules (Fig. 2), were added. Adhesion was verified by dragging the beads with a single beam optical tweezers. The tweezers could stretch or buckle the microtubules via the beads (Fig. 3), showing that the beads were attached to a single point and could not roll or slide.

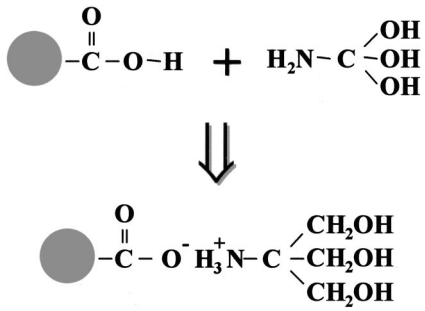

FIG. 2. Microspheres (beads) are activated chemically [59] in order to adhere to the microtubule filaments. The carboxyl functionality of the bead reacts with the amine of the tris (hydroxymethyl) aminomethane, usually referred to as ''tris'' or ''trizma'' buffer, to form an ionic bond. The newly functionalized bead adheres to the microtubule via multiple hydrogen bonds.

The observation consists of recording the bead motion for extended time periods. A small region of interest surrounding a single bead is captured at a frequency up to the video frame rate into the disk of a personal computer. A ''mask'' image is taken of the bead itself, and then a cross-correlation algorithm (Inspector 1.7, Matrox Imaging, Quebec, Canada) is run in order to locate the instantaneous position of the bead in each frame. The raw data are thus a list of coordinates for the projection of the bead, and a corresponding counter specifying the frame number $i=1,2,\ldots,N$. The original (x_i,y_i) list is then rotated in small steps and the process repeated so as to align the measurement to the transverse and longitudinal axes of the microtubule (h_i,v_i). The trajectory of the transverse motion of the bead (h_i) is used to compute the undulatory mean square displacement vs time. Because the process is stationary, the MSD can be computed as a time average for a single trajectory, rather than an ensemble average,

FIG. 3. Differential interface contrast (DIC) image showing a microtubule (indicated by the arrows) to which three 0.3 μm beads were attached. Single beam optical tweezers were used in order to buckle the microtubule by applying force on the right-most bead that was attached to the filament. DIC optics based on $\times 100/1.3$ NA objective (Zeiss), allows the simultaneous observation of the beads and the microtubules. The optical tweezers are based on an 830 nm single-mode laser diode with a maximum power of 200 mW (SDL-5432-H1, SDL Inc., San Jose, CA). The horizontal dimension of the figure is 20 μm.

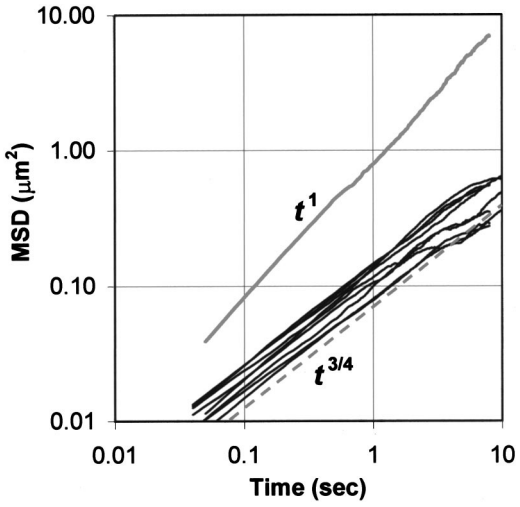

FIG. 4. Measured results of the transverse MSD [$\langle h^2(t)\rangle$] of a 0.3 μm bead attached to a point along the MT filament shown using *thin black lines* for ten different samples. The *dashed gray line* shows the expected MSD according to Eq. (5). As a reference a measured MSD for a 0.3 μm bead in a sucrose solution (33% by weight) is shown by *gray line*.

$$\langle h^2(n\Delta t)\rangle = \frac{1}{N-n-1}\sum_{i=1}^{N-n-1}(h_{i+n}-h_i)^2, \qquad (6)$$

where Δt is the time difference between successive position measurements, in our case 40 ms. Measured results from several cases are shown in Fig. 4, along with the calculated MSD for a MT filament taking a persistence length of 6 mm, calculated from the full equation for the MSD given in Ref. [26]. The data clearly show the anomalous exponent of 3/4.

IV. SEMIFLEXIBLE POLYMER NETWORKS

Within a network of semiflexible polymers, a particle larger than the typical distance between filaments is effectively caged and performs a restricted diffusion due to collisions with the surrounding filaments. Recently, many experiments have observed the thermal motion of embedded particles in order to study the bulk properties of complex fluids such as biopolymers. Studies of this type are usually called microrheology [29]. Observations have been made on thermal motion in polymer networks, either of a single particle averaged in time [30], of the average of the motion of many particles [31], or on the cross-correlated motion of pairs of particles [32]. It was shown, by video tracking, that a particle embedded in a network of F-actin with a diameter larger than the mesh size executes a subdiffusive motion with an exponent of 3/4 [30]. This scaling law is equivalent to that of a point along the filament but has alternately been explained in terms of gel rheology [33]. The results of the particle studied, within a network, are in agreement with earlier light scattering measurements [34]. Using high bandwidth laser tracking, it was shown that the shear modulus of a semiflexible solution has high frequency scaling of $\omega^{3/4}$, in contrast to $\omega^{1/2}$ scaling for flexible semidilute polymer solutions [35]. Using diffusive wave spectroscopy it was possible to detect the $t^{3/4}$ scaling over many decades in time [36,37].

The anomalous diffusion, discussed above for a particle within a network, indicates that the network environment is not a simple viscous medium. In a Newtonian fluid it is possible to define the diffusion constant as $k_BT/6\pi\eta a$ where $6\pi\eta a$ is the coefficient of the viscous friction. Within a network of semiflexible polymers, different time scales access different spatial modes of the filaments. A particle driven through the network by an external force locally disturbs the geometry of the surrounding filaments. This local perturbation is composed of many modes in each filament, each having a different time decay. The $t^{3/4}$ scaling measured on the thermally driven motion can be used to define a time-dependent friction with a scaling of $\mu_e(t)\sim t^{1/4}$. A driven process in such a non-Newtonian environment will be subject to the same time-dependent friction. As a consequence, one may expect that under constant force the motion of a driven particle will be depressed by the network and the displacement will not be linearly proportional to time but rather to $t^{3/4}$ [30,38].

V. VISCOELASTICITY IN LIVING CELLS

Several experimental works have been conducted in order to study the complex rheological environment of the cytoplasm inside living cells. Using size-fractionated Ficoll, with radius of gyration between 3 and 58 nm, it was shown that diffusion inside the living cell is hindered in a size-dependent manner [39]. It was also shown that within the cell the diffusion constants obtained from direct single molecule tracking of different trajectories has a broader distribution than the narrow distribution in a simple viscous fluid [40]. The results of the above experiments raised a question regarding the meaning of the diffusion constant, which is defined for thermal systems within a simple medium, to the living cell. Measurement using fluorescence correlation spectroscopy also showed that the motion of single molecules is not consistent with simple Brownian diffusion, and two models were proposed [41]. The first model regards two components for the motion in which one fraction of the molecule diffuses faster than the other. The second model is based on hindrance to the motion by obstacles that result in anomalous power law scaling of the diffusion.

Using engulfed magnetic beads, the viscoelasticity inside living J774 macrophages [42] or *Dictyostelium* cells [43] was obtained by measuring the probe response as a function of an applied magnetic field. It was shown that the viscoelasticity is very heterogeneous and its value varies depending on the applied force. Twisting of such beads has also been used to study the viscoelastic response of the cytoplasm, particularly in combination with drugs that cause specific depolymerzation of F-actin or microtubules [44]. The fact that force is required for twisting the magnetic sphere supports the hypothesis that the bead is strongly coupled to the elastic filaments that construct the intracellular network.

In addition to the measurements that use an engulfed bead as a probe, microrheological experiments have also been conducted on lipid granules naturally present in some cells.

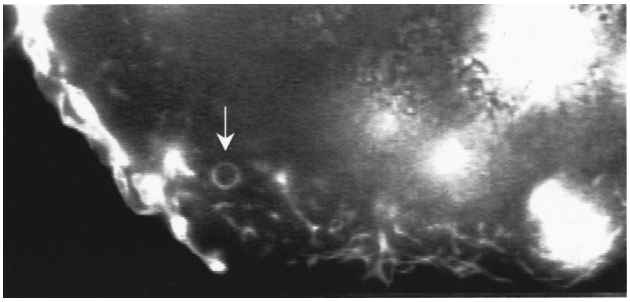

FIG. 5. Immunofluorescence image showing the membrane shell around an engulfed bead marked by the *white arrow*. A live SV80 cell was stained using a membrane-specific fluorescent dye (CellTracker CM-DiI, Molecular Probes, Eugene, OR), after placing a 3 μm bead at the cell periphery with the optical tweezers.

Using laser tracking microrheology [45] the motion of a single lipid sphere can be tracked vs time. Viscoelastic shear moduli were measured at various locations inside the cell, before and after depolymerization of the actin network [46].

VI. ANOMALOUS DIFFUSION IN LIVING CELLS

A particle engulfed into a living cell can act as a reporter probing the microrheological properties of the cytoskeleton. Clearly, the interaction of the particle is not only due to the thermal collisions. Dynamic processes such as the interaction with motor proteins must be considered and may be dominant. Using the membrane specific fluorescent dye DiI, we found that a particle engulfed into a cell is covered by a membrane shell (Fig. 5). The presence of this shell is due to the process by which the particle is ''cupped'' by the cell cortex leaving it surrounded by a layer of plasma membrane [1]. This process is similar to phagocytosis, by which many cells ingest external materials. Thus, from the point of view of the cytoskeleton network, the bead is likely to be recognized as a membrane-bound vesicle or digestive organelle. Within the cell the vesicles are transported by adsorbing motor proteins on their surface, and move back and forth along the microtubles [47].

Experiments were performed on cells of the human derived SV80 line [48], with some on multinuclear giant cells [49] of the same line, and others on murine NIH-3T3 cells. Cells were cultured at 37 °C in Dulbecco's Modified Eagle Medium at 7.5% CO_2 with 10% fetal calf serum in petridishes with glass bottoms. The medium was exchanged for L-15 (CO_2-free medium) prior to observation and the sample maintained at 37 °C during experiments. Observation was made using an inverted optical microscope equipped with an oil-coupled Fluar $\times 100/1.3$ numerical aperture objective (Carl Zeiss, Germany) and a 1/2 in. charge-coupled-device video camera with $0.5\times$ reducing lens (160 nm/pixel). Bright field imaging was used for particle tracking while differential interface contrast was best for cell observations. Image sequences from the video camera were captured directly to the disk of a personal computer at the video rate (25 frame/sec).

Polystyrene beads, 3 μm in diameter (Polyscience, Warrington, PA; Interfacial Dynamics Corp., Portland, OR), were

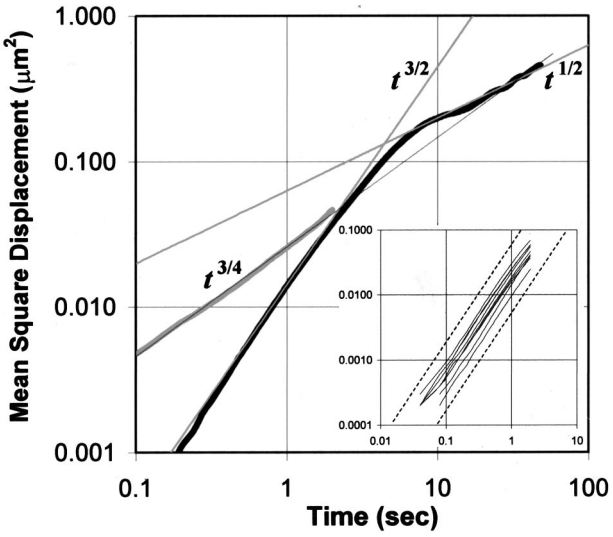

FIG. 6. Crossover between $t^{3/2}$ scaling and $t^{1/2}$ scaling of the measured MSD of a 3 μm bead engulfed within the SV80 cell—*black line*. Subdiffusive motion with $t^{3/4}$ scaling measured for a granule naturally appears in the same cell line—*gray line*. Thin guidelines represent power law scaling as indicated. Inset shows the measured MSD for ten different samples at short times, <2 sec. The broken guidelines represent power law scaling of $t^{3/2}$.

introduced into the cells either by incubation with the cell culture during replating, or by direct placement on the cell periphery using optical tweezers. The beads were coated on their surface by the lectin concanavalin A (Sigma, cat. no. C-7275) so as to adhere to the cell membrane. (Untreated sulfate beads also successfully adhered to the cells.) The adherent particles were engulfed into the cell volume and carried to the central part of the cell, near the nucleus. All measurements presented here were made in this central part of the cell. We verified by scanning electron microscopy as well as live observation with three-dimensional particle tracking, that the beads are engulfed into the cell volume rather than adhering to the outer surface of the cell [1].

The measurements consist of recording the bead's motion and calculating the MSD. The results show two distinct time regimes (Fig. 6). At short times ($t<1$ sec), we observe enhanced diffusion $\langle x(t)^2\rangle \sim t^{\gamma}$, where $\gamma \approx 3/2$. Twenty-four different measurements yield $1.38<\gamma<1.56$, with an average of 1.46 and a standard deviation of 0.06. At long time scales ($t>1$ sec), we observe subdiffusive motion with an exponent $0.5<\gamma<1$. We never observed an exponent less than 1/2. Such different scaling at different time regimes of the mean square displacement gives a measure of the time scale of the interactions within the system.

The short time regime is limited to a specific time scale. Measuring at very short times will probe the individual step length of the driving process, as seen for example in *Listeria* movements within a living cell [50]. On the other hand, the upper limit is determined by the crossover to a different behavior at a time interval of a few seconds. Thus, the temporal resolution of video particle tracking matches the time scale regarding the collective activity of motor proteins within the cell. However, the error in determining exponents increases for a decreasing time span. We estimate as follows the error

in the above exponents, which were measured over one and half decades. First, we estimate the error of the mean square displacement at the edge of the time domain, i.e., at 0.04 and 1.0 sec. A common way to estimate the error for a mean of sampled data is the standard deviation divided by square root of the number of samples [51]. Second, we estimate the error of the exponent by calculating the power law based on extreme values of the MSD at the edge of the time regime. Using the above we estimate the error on the measured power law to be 0.06.

Calculating MSD at long times requires acquisition of very long sequences [52], and it is risky to fix exponents at such time regimes. Because the MSD is computed as a time average for a single trajectory, Eq. (6) assumes that $n \ll N$. We typically acquired sequences of 8 min duration ($N = 12\,000$ frames), and for each experiment the MSD was calculated on various time windows sampled from the long sequence. We began by calculating the MSD using all 12 000 frames. Next the MSD was calculated separately from the first and last 6000 frames. Finally, the MSD was calculated on three successive windows, each of 4000 frames. The MSD evaluated from all time windows gave similar results until 48 sec ($n = 1200$ frames). In many of the resulting analyses the scaling at long time clearly shows a crossover to a subdiffusive regime. We further note that this crossover takes place at MSD values much smaller than what we would expect due to confinement of the bead to a restricted box, i.e., a particular location within the cell. Within a box the MSD saturates at a value of $\frac{2}{3}L^2$, where L is the box size. In our case the bead wanders within a space larger than its diameter, and therefore saturation would be expected at amplitudes greater than 6 μm^2. In fact the crossover we observe takes place at much smaller amplitudes, (e.g., 0.3 μm^2 for the case shown in Fig. 6).

The engulfed bead could easily escape a single beam optical trap, while the same trap could hold stationary a bead subject to a Stokes drag force of as much as 120 pN. Taking into account that the stall force of a single kinesin motor is about 5 pN, the inability of the optical trap to hold the engulfed particle clearly indicates the simultaneous activity of many motors. The motion of the particle suggests that the motor system moving the bead is stochastic. The bead shell may adsorb kinesin and dynein randomly, which results in a randomly driven wandering motion. Moreover, there may be sufficient local disorder within the microtubule array to generate a random path even with a single motor. The force scale is in agreement with a recent study using magnetic beads [43]. There, it was shown that the implanted probe moves in directions other than that of the applied force, indicating the involvement of internal forces. Analyzing the change in the velocity vector relative to the applied force yielded an active internal force of 200 pN upon a micron-sized bead.

In principle, the driven motion could be a result of actin-myosin motors or microtubule-associated motors. Using various drugs we can disrupt the filament systems specifically. Incubating the cell culture with 10 μM nocadazole (Sigma, cat. no. M-1404) for 5 h, destroys the microtubule network and leaves the associated motor proteins without an extended track along which to move. The actin network can be disrupted by treatment with 2 mg/ml cytochalasin D (Sigma, cat. no. C-8273) for 2–3 h. Nocodazole-treated cells show a loss of long range internal vesicle movements, while cytochalasin-treated cells are unable to divide. The depolymerization of the microtubule network eliminated the enhanced diffusion, while actin depolymerization had no measurable effect on the MSD scaling [3]. Thus, we may conclude that the microtubule-associated motor system is responsible for the enhanced diffusion and associated anomalous power law, $\langle x^2(t)\rangle \sim t^{3/2}$.

Active transport in a purely viscous medium may result in a crossover from ballistic to diffusive motion. Suppose that a particle is actively transported in a purely viscous medium by a stochastic force whose mean is vanishing, and whose correlation function obeys: $\langle F(t_1)F(t_2)\rangle = \langle F^2\rangle e^{-|t_1-t_2|/\tau}$, where τ is a characteristic correlation time. Unlike thermal forces the active force is not subject to the fluctuation-dissipation theorem. The equation of motion $\dot{x}(t) = v(t) = F(t)/\mu$, where μ is the frictional drag, leads to the following MSD:

$$\langle x^2(t)\rangle = 2\langle v^2\rangle \tau[t - \tau(1 - e^{-t/\tau})]. \tag{7}$$

At short times this reduces to a quadratic scaling of the MSD, i.e., the *ballistic regime*, $\langle x^2(t)\rangle = \langle v^2\rangle t^2$ where $\langle v^2\rangle = \langle F^2\rangle/\mu^2$. At times longer than the characteristic correlation time, this equation reduces to linear scaling, i.e., the *diffusive regime*, $\langle x^2(t)\rangle = 2Dt$, where $D = \langle v^2\rangle \tau$.

A ballistic regime with expanded time scale was recently demonstrated using a large bead embedded in a two-dimensional bath of bacteria [6]. The bead is driven by random impulses, as each bacterium swims in a particular direction for a short time and the collective activity upon the bead is random. The measured MSD on such a particle shows a superdiffusive regime at short times, with an exponent between 1.5 and 2, and normal diffusion at longer times. The measurements can be fit successfully to the above equation, suggesting that the observed scaling represents a crossover from ballistic to diffusive regimes. In order to exclude the possibility that the enhanced diffusion we observe may be a crossover regime, we checked that our measured data cannot be fitted to Eq. (7). Moreover, the exponents smaller than 1 measured at long time scales are not consistent with a simple crossover from ordinary ballistic to diffusive motion.

The non-Newtonian environment inside the cell suggests an explanation for the anomalous diffusion based on hindrance to ballistic motion. The origin of the hindrance lies in the polymer response. This response was observed under thermal excitation in the experiments using purified biopolymers. During its motion the bead must deform the microtubule network. Thus, the time-dependent friction in the cytoplasm depresses the scaling of the ballistic motion inside the cell. This hypothesis is also consistent with the subdiffusive motion observed for nondriven lipid spheres (granules) naturally appearing in these cells. As the passive diffusion of the intracellular granules or beads in a network of purified polymers is subdiffusive, the driven motion of the engulfed beads will be subballistic.

VII. TIME-DEPENDENT FRICTION

The above proposal can be discussed in the context of the Einstein relation between thermal and driven processes. The two-dimensional MSD $\langle x^2(t)\rangle_{TH}$ measured in thermal, i.e., nondriven environments such as lipid granules or beads embedded in motorless networks, defines an effective time-dependent friction

$$\frac{4k_BT}{\mu_e(t)}=\frac{d}{dt}\langle x^2(t)\rangle_{TH}. \tag{8}$$

For simple Brownian diffusion this yields the scalar Newtonian viscosity, whereas subdiffusive motion implies time-dependent friction. In our case the scaling yields $\mu_e(t)\sim t^{1/4}$. We can use this scaling in order to calculate the expected scaling of the MSD of a particle embedded in the same non-Newtonian environment with the presence of applied force $\langle x^2(t)\rangle_F$. As discussed above, the motor proteins drive the bead randomly in different directions, within a limited region in the cell. Thus the force upon the bead is randomly distributed between positive and negative values, with vanishing mean on long time scales but with finite variance $\langle F^2\rangle$. Since the driven velocity is $v(t)=F/\mu_e(t)$, one finds that the MSD in the presence of a random driving force is

$$\langle x^2(t)\rangle_F=\frac{\langle F^2\rangle}{(4k_BT)^2}\langle x^2(t)\rangle_{TH}^2. \tag{9}$$

A more accurate approach is formulated in the framework of the generalized Langevin equation [53–55]

$$\int_0^t \mu(t-t')v(t')dt'=F(t)+\zeta(t). \tag{10}$$

Here $\mu(t)$ is a memory friction and $F(t)$ is the external driving force [note that $\mu(t)$ and $\mu_e(t)$ are not equal and do not have the same dimensions, see Eq. (13)]. $\zeta(t)$ is the thermal noise obeying the fluctuation-dissipation theorem, which relates its correlation function to the friction by

$$\langle\zeta(t)\zeta(t')\rangle=k_BT\,\mu(t-t'). \tag{11}$$

For simple Brownian diffusion $\mu(t-t')=\delta(t-t')$, i.e., the friction has no memory.

First we consider the nondriven case $[F(t)=0]$. In Laplace space we obtain the generalized Einstein relation [56],

$$s^2\langle x^2(s)\rangle_{TH}=\frac{4k_BT}{\mu(s)}. \tag{12}$$

Comparing to Eq. (8) we find the relation between the two friction coefficients,

$$\mathcal{L}\left[\frac{1}{\mu_e(t)}\right]=\frac{1}{s\mu(s)}, \tag{13}$$

where $\mathcal{L}[g(t)]$ denotes the Laplace transform of the function $g(t)$. Second, we can use the friction obtained by Eq. (12) to find the MSD in the case of a particle driven by an external force in a medium characterized by $\mu(s)$. The Langevin equation in Laplace space can be written as

$$sx(s)=v(s)=\frac{F(s)+\zeta(s)}{\mu(s)}, \tag{14}$$

which yields the solution for the driven case as a function of the applied force and the MSD of a *nondriven* probe in the same environment

$$\langle x(s)\rangle_F=\frac{sF(s)}{4k_BT}\langle x^2(s)\rangle_{TH}. \tag{15}$$

For a stochastic force, such as the force exerted upon the engulfed bead by the collective activity of motor proteins, at times shorter than the correlation time of the force the above equation yields Eq. (9). In our case the $t^{3/4}$ power law measured for the thermally driven particles leads to $t^{3/2}$ scaling, as measured for the cell-engulfed beads. The response of the intracellular network depends on its memory of the impulse duration, rather than just on the instantaneous velocity.

Consider now long times relative to the correlation time of the force. In the case of time-dependent friction the MSD is given by

$$\langle x^2(t)\rangle_F=\int_0^t\int_0^t\frac{\langle F(t_1)F(t_2)\rangle}{\mu_e(t-t_1)\mu_e(t-t_2)}dt_1dt_2. \tag{16}$$

Taking $\langle F(t_1)F(t_2)\rangle=\langle F^2\rangle e^{-|t_1-t_2|/\tau}$ implies that for $t\gg\tau$, where the driving force is decorrelated, $\langle F(t_1)F(t_2)\rangle=\langle F^2\rangle\tau\delta(t_1-t_2)$, the MSD is

$$\langle x^2(t)\rangle_F=\int_0^t\frac{\langle F^2\rangle\tau}{[\mu_e(t-t_1)]^2}dt_1. \tag{17}$$

For our case the friction has time scaling of $\mu_e(t)\sim t^{1/4}$ and we get

$$\langle x^2(t)\rangle_F\sim t^{1/2}. \tag{18}$$

VIII. MSD SCALING vs BEAD SIZE

The above considerations presume that the bead maintains intimate contact with the microtubule network, so that in order for it to move it must push the surrounding filaments out of the way. In order to check whether the anomalous $t^{3/2}$ scaling depends on such contact between the bead and the microtubules we used beads of various sizes. Similar experiments could in principle be made using a sparse network. However, practically it is problematic to control the network density within the living cell. We may expect that smaller beads will have rarer interactions (Fig. 7) with the network and their motion will approach normal ballistic scaling, i.e., a larger exponent approaching 2. In the case of a passive network, it was shown that beads smaller than the mesh size perform ordinary diffusion while larger beads, which are locked in the network, perform subdiffusive motion [30]. It was also demonstrated that instantaneous velocities of small beads (0.5 μm diameter) engulfed into *Dictyostelium* cells

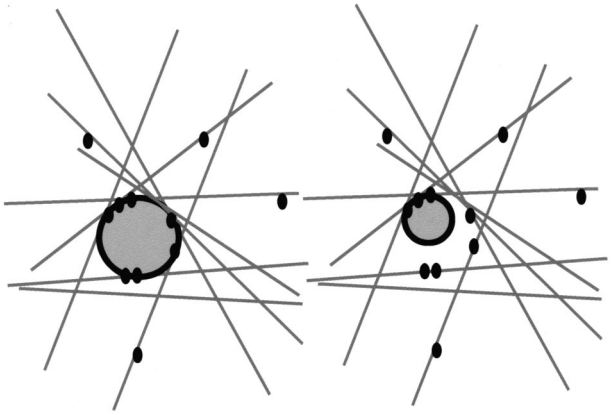

FIG. 7. Cartoon of the cage formed by the MT network for small and large beads. A small bead can diffuse or rattle within a limited area while a large bead must push the surrounding filaments out of the way in order to move. *Solid lines* represent the MT filaments. *Small dots* represent the motor proteins, and the *black shell* represents the membrane surrounding the bead.

are higher than for larger beads (1.5 μm diameter) [43].

Experiments measuring the MSD of the random wandering motion within the cell, as described above, were conducted for beads with diameters 1, 2, and 3 μm. Results from typical cases measured inside SV80 cells are shown in Fig. 8. At short times we have observed enhanced diffusion; the mean square displacement $\langle x(t)^2 \rangle$ is proportional to t^{γ} with $\gamma > 1$, for all bead sizes. The 3 μm bead used previously [3] performs an enhanced diffusion with an exponent of $\gamma = 1.46 \pm 0.06$ (24 samples). The same scaling was measured also for 2 μm bead diameter, $\gamma = 1.47 \pm 0.03$ (3 samples). However, the 1 μm diameter beads display a scaling with a lower exponent of $\gamma = 1.33 \pm 0.10$ (18 samples) and broader distribution. (Data are given as an average $\pm$ standard deviation over the number of samples specified.) Thus, the larger beads yield an exponent of 3/2, while the smaller beads also perform an enhanced diffusion but with a lower apparent exponent.

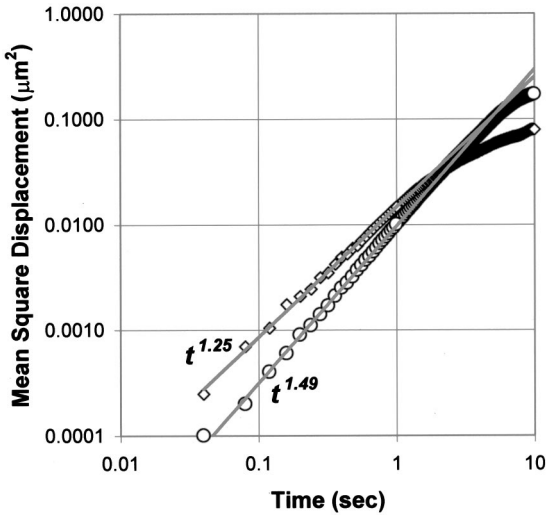

FIG. 8. Measured MSD for 1 μm bead (diamonds) and 2 μm bead (circles), inside an SV80 cell. *Solid gray lines* are fits over the short times regime (<1 sec). For the 1 μm bead, the chart shows a case with relatively low exponent (1.25, vs an average of 1.33) in order to highlight the change compared to the 2 μm bead diameter.

We would like to check whether the anomalous diffusion measured above for various beads relates to the density of the network in which the bead is embedded. Using the weak force of the optical tweezers we tried to move the engulfed bead. The optical tweezers are much stronger than thermal diffusion, so a particle that cannot be moved by the optical forces also cannot diffuse by Brownian motion. In order to quantify the ability of the engulfed bead to be moved by the optical tweezers, we scanned the tweezers relative to the bead at a low frequency (0.2 Hz) and measured the deflection of the bead position. We refer to this as ''rattling.'' Two detection techniques were used. The first was based on video tracking and the second on a two-photon fluorescence technique. These will be described separately in the following sections.

IX. RATTLING—VIDEO TRACKING

Using optical tweezers we ''rattled'' the engulfed microsphere. The restricted volume in which the optical forces can drag the bead gives a measure of the free space available for the bead to move. An experimental setup was built around a standard inverted microscope equipped with an oil-coupled Fluar objective $\times 100/1.3$ (Carl Zeiss, Germany) and a stage driven by closed-loop piezoelectric positioners (Physik Instrumente, Germany). The optical trap is based on a solid state 983 nm infrared Master Oscillator Power Amplifier laser, with maximum power output of 1 W (SDL-5762-A6, San Jose, CA), whose output is steered and expanded ($\times 2.5$) before being introduced to the microscope via the epifluorescence port. A dichroic mirror (750DCSP, Chroma Technology, Inc.) directs the laser into the objective. We aligned the optical trap to be stationary at the center of the field of view and scanned the sample back and forth. We followed the location of the bead, during the scanning, using standard video tracking as described above.

The stage was scanned with peak-to-peak amplitude of 17.5 μm at a frequency of 0.2 Hz. In case the bead was embedded in a solution with a viscosity equal to that of water, the drag force upon it will be 0.07 pN and 0.21 pN for 1 μm and 3 μm beads, respectively. Experiments were carried out with a laser output power of 400 mW. At such a power the escape force from the tweezers, measured by Stoke's drag in water was 15 pN for the 1 μm bead and 48 pN for the 3 μm bead. Thus, under the above scanning conditions the optical tweezers could hold the bead against the Stokes drag even in a solution 200 times more viscous than water.

During measurements the entire stage, with the cell and the bead engulfed within it, is scanned relative to the optical tweezers. When the bead arrives near the optical axis it drops into the trap and is dragged until drawn out due to collision with a hard material, most likely the cytoskeleton, which is the only nonfluid material in the cytoplasm.

In order to measure the distance by which the tweezers

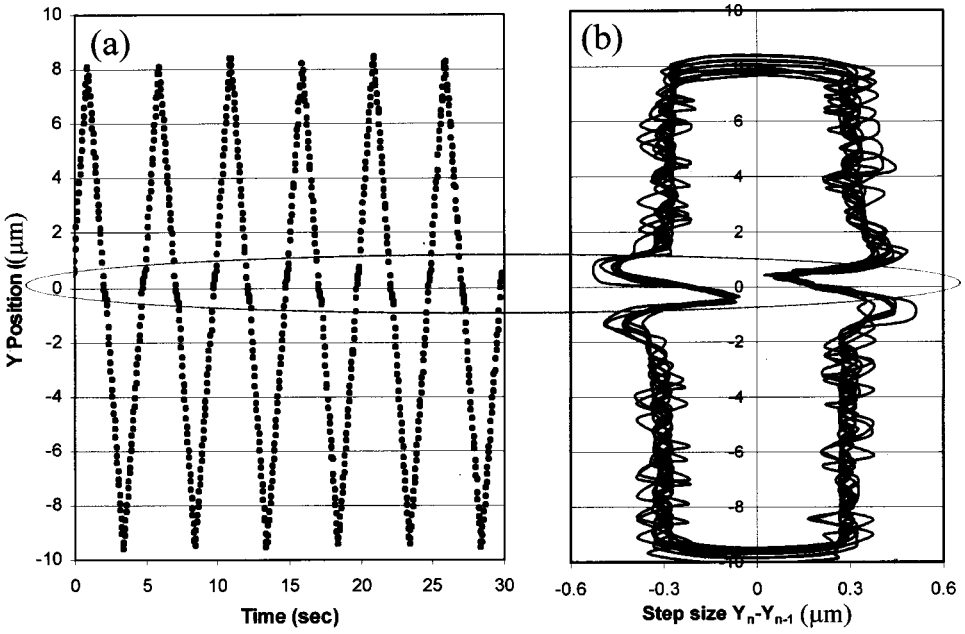

FIG. 9. Rattling of a 1 μm bead inside a living SV80 cell. (a) Position vs time as measured by video tracking. (b) The difference in the bead position between successive frames as a function of the bead position (''graphic average'').

can move the bead we calculate the difference in the bead position between successive video frames. Where the tweezers have no effect on the motion, this difference is a positive/negative constant dependent on the scanning direction and velocity. In case the tweezers can trap and hold the bead, the difference in successive positions is close to zero. In order to eliminate noise in the particle tracking and other sources of movements such as kicks from the motor proteins, we average the difference between bead position over several cycles. Data are presented in a ''graphic average'' by plotting the difference in the bead position between successive frames as a function of the bead position. Such a chart easily shows the periodic change in the motion of bead.

Rattling of 1 μm and 3 μm engulfed beads show different behaviors. A 1 μm bead could be moved within a space of ≈ 2 μm length (Fig. 9). By contrast, the optical tweezers could only slightly move the 3 μm bead (Fig. 10). We also measured the MSD of 1 and 3 μm beads that were subject to the above rattling experiments. The results are consistent with the data presented earlier. For the 3 μm bead we found power law scaling at short times with an exponent of $\gamma = 1.48 \pm 0.07$ (five cases). For the 1 μm bead we measured an exponent of $\gamma = 1.36 \pm 0.06$ (four cases). The ability to rattle under optical forces was therefore found to correlate with the lower exponent measured for its wandering motion.

As pointed out above, the bead is pulled out from the trap because it collides with the intracellular network. Motion at the scale of the bead diameter, as observed in the wandering movement showing enhanced diffusion, can be achieved only if the cytoskeleton network is deformed. Forces much larger than those provided by the optical tweezers are re-

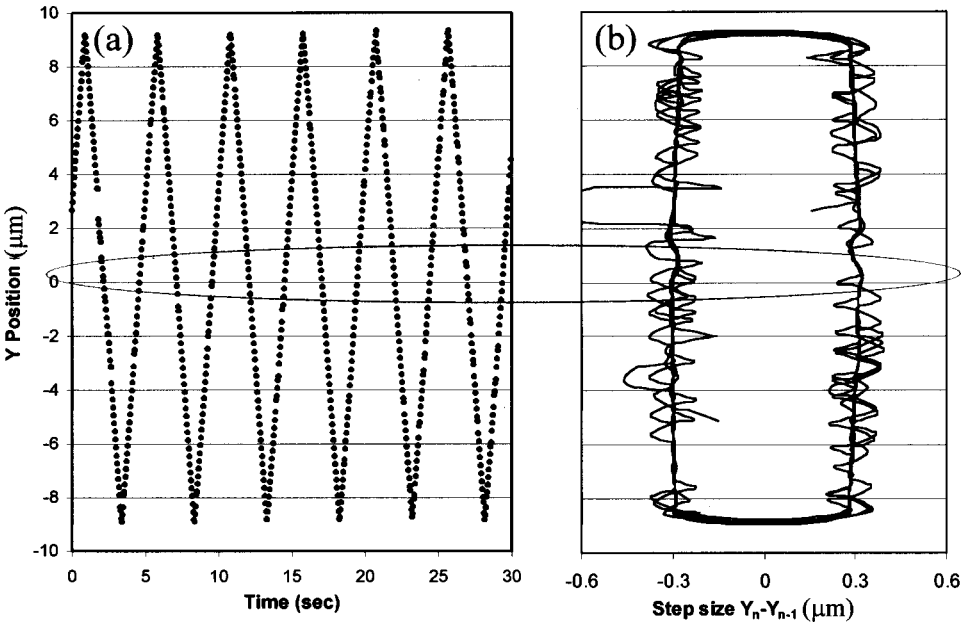

FIG. 10. Rattling of a 3 μm bead inside a living SV80 cell. (a) Position vs time as measured by video tracking. (b) The difference in the bead position between successive frames as a function of the bead position (''graphic average'').

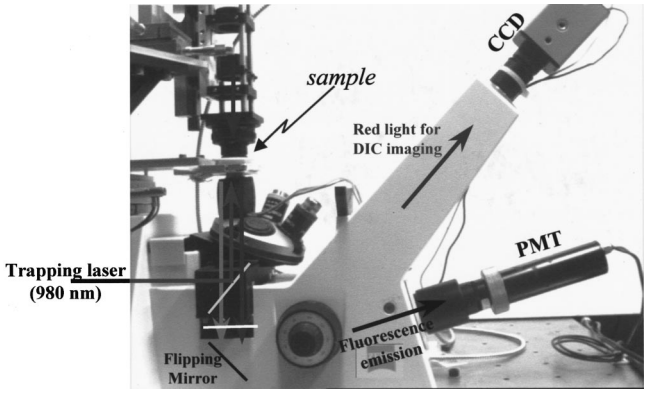

FIG. 11. A picture of the experimental setup used for the two-photon measurements.

quired. For inducing forced movement a different driver is needed such as magnetic tweezers or direct mechanical manipulation. Thus, the observed wandering movement observed clearly indicates collective activity of motor proteins. Depolymerization of the microtubule network by nocodazole allowed the bead to be dragged freely inside the cell (data not shown).

X. RATTLING—TWO PHOTON

Particle tracking inside the living cell using video based techniques is limited in part because it is difficult to distinguish between a bead and vesicles or granules that appear naturally in the cell. The problem becomes more critical when smaller beads are used. Fluorescent beads are easy to distinguish, but require illumination of the cells with strong visible light. This is known to have deleterious photochemical effects. We have developed a different method in which the probe acts as a source of light rather than an imager or a scatterer. The same infrared laser beam used for the optical tweezers also excites fluorescence in the bead by a continuous-wave two-photon absorption process [57]. Excitation occurs optimally when using a fluorescent bead that has an excitation maximum around half of the wavelength of the trapping beam. As the bead is pulled away from the optical trap the fluorescence intensity decreases. Thus the emitted intensity gives a measure of the position of the bead relative to the optical axis without using particle tracking. A similar methodology has been used as a scanning microscope for mapping surface topology [58]. We used this setup for mapping the internal cage of the network.

The experimental setup is built around a standard inverted microscope (Fig. 11) with the same scanning stage and optical tweezers described above. The 983 nm trapping laser efficiently excited beads having excitation maximum at 488 nm or 505 nm. Experiments presented here used yellow green fluorescent beads [F-8823 (1 μm) and F-8853 (2 μm), Molecular Probes, Eugene, OR]. Fluorescence emission was measured by a photon-counting photomultiplier unit (H6180-01 Hamamatsu, Japan), mounted at the microscope camera port. The faceplate of the detector was placed behind the image plane in order to distribute the light intensity. Pulses corresponding to photon arrivals were measured using a gated photon counter (SR400 Stanford Research Systems, Sunnyvale, CA). The analog output of the counter was sampled using an acquisition board (PCI-1200 National Instruments, Austin, TX).

We compare the rattling and MSD between 1 and 2 μm beads. (As pointed out above, we found no measurable difference between the power law scaling of 2 and 3 μm beads, and the most intensely fluorescent beads are unavailable in 3 μm diameter.) The stage is scanned back and forth while the optical tweezers are located at the origin. When the bead comes close to the optical axis, where the tweezers are located, the optical trap holds the bead for a certain period of time, during which the fluorescence intensity is high. This duration represents the restricted length in which the bead can be moved. Of course, when the bead is not held by the tweezers, the emitted intensity is zero and the counter output is the dark count of the photomultiplier tube. A fixed bead will be subject to the excitation from the laser for a short period, while a bead in a box will be excited for a duration in accordance with the size of the box. By comparing the intensity vs position for scanning around a cell-engulfed bead to scanning around a fixed bead, we measure the length on which the bead can be rattled within the intracellular network.

First we scanned the stage back and forth around a bead fixed to the coverslip, and measured the emitted fluorescence as function of the stage position (Fig. 12, gray lines). Second, we scanned the stage back and forth around a bead engulfed into the cell, and we plotted the emitted intensity vs stage position (Fig. 12, black lines). As can be seen from Fig. 12, the 1 μm bead could be rattled by the optical force while the 2 μm bead could not be moved by the tweezers. The intensity profile of the 2 μm bead inside the cell is almost identical to the profile of a fixed bead, indicating that the bead is locked inside the cage formed by the cytoskeleton network. In contrast, the intensity profile of a 1 μm bead inside the cell is wider than the profile measured on a fixed bead. In accordance with the video based measurements, the 1 μm bead could be moved by the modest force of the tweezers and may also diffuse inside that cage. Measurements were carried out on five different samples for each bead diameter. Again we measured the MSD of the wandering motion for the 1 and 2 μm beads before and after the rattling. For the particular cases shown in Fig. 12, we found an exponent of 1.49 for the 2 μm bead and an exponent of 1.34 for the 1 μm bead.

XI. SUMMARY AND DISCUSSION

The measured anomalous scaling for the MSD of a cell-engulfed probe, $\langle x(t)^2 \rangle \sim t^{3/2}$, is explained based on the subdiffusive scaling observed for microtubule undulations *in vitro*. Within a semiflexible polymer network it was shown, by us as well as by others, that a nondriven probe performs a subdiffusive motion with $t^{3/4}$ scaling. Using the generalized Einstein relation we were able to connect this to other observations in the living cells. Driven motion of the probe within the cell deforms the surrounding microtubule network, pushing other filaments out of the way. These deformations ac-

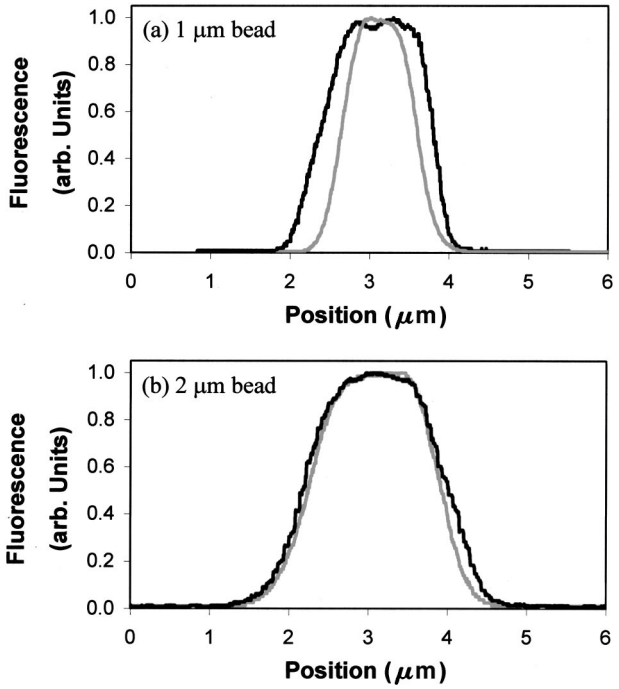

FIG. 12. Two-photon fluorescence intensity vs position when scanning around an (a) 1 μm bead, and (b) 2 μm bead. *Black lines*—scanning around an engulfed bead that may be dragged for a short period within the cell by the optical tweezers. *Gray lines*—a reference bead fixed to the cover slip in a solution of phosphate buffered saline with high salt concentration ($\times 10$). A bead was trapped by the optical tweezers and lowered until it touched the surface of the cover slip. In such a high-salt solution the bead adheres to the glass immediately due to van der Waals forces, and cannot be moved away by the optical forces.

cess many bending modes of the surrounding filaments, whose elastic properties determine the microrheological response. As each bending mode of the microtubules has a wavelength-dependent damping rate, the effective drag on the driven probe acquires a time dependence. This leads to $t^{3/2}$ scaling at short times, crossing over to $t^{1/2}$ scaling at long times, in agreement with the observations.

The above argument depends on the intimate contact between the probe and the surrounding microtubules. Rattling beads with different sizes using optical tweezers within a living cell shows that a 1 μm diameter bead can be moved by the weak optical forces, in contrast to 2 and 3 μm beads that cannot be moved. All the engulfed beads studied perform an enhanced diffusion, i.e., $\langle x(t)^2 \rangle \sim t^{\gamma}$ with $\gamma > 1$. For the beads that could not be rattled by the optical tweezers, i.e., 2 and 3 μm beads, we found that $\gamma = 3/2$, in agreement with the prediction of the generalized Einstein relation. For smaller beads that could be rattled by the optical tweezers, i.e., 1 μm diameter, smaller and more broadly distributed apparent values of γ are observed.

Given that the larger beads could not be moved by the optical forces, they must deform the crowded cytoskeleton network in order to move. That can be achieved only by a driven force of the motor proteins and not by Brownian motion. Thus, the wandering motion of the large beads is composed only of directed forces larger than the escape force of the optical tweezers, most likely a collective activity of many motors operating simultaneously. The 1 μm beads, however, could be rattled and therefore may move without external force or motors in a restricted cage within the network. Hence, the wandering motion of the 1 μm bead may be composed of a thermal component in addition to the random kicks of the motor proteins, resulting in a lower exponent.

It remains possible that in the case of the smaller bead, i.e., a sparse network, the bead is attached to a single filament. The attached bead is rattled because the optical tweezers can buckle single microtubules. This bead can also diffuse due to the transverse undulation of the filament. In such a case, when turning off the driving motor we would expect an MSD with $t^{3/4}$ scaling. Unfortunately, within the cell it is impossible to turn on and off the driving forces. Experiments within more controllable systems such as cell extracts may be used in order to check the suggested models.

The current work implements the approach of microrheology and particle tracking studies made on purified cytoskeletal networks to the living cell. In contrast to experiments tracking the dynamics of single molecules or small vesicles within the cell, our probe is large, comparable in diameter to the mesh size of the network. Moreover, the probe is driven by the collective activity of motor proteins, as indicated by the inability of the optical tweezers to stop its wandering motion. The properties of those motors have been extensively studied in clean and controllable *in vitro* systems. Within the cell, motors may operate stochastically and hence the net effects of the motors cannot be described simply by force and velocity, but statistical parameters such as mean square displacement should be considered. As shown here, these may reveal interesting properties of the intracellular environment.

ACKNOWLEDGMENT

This work was supported in part by a grant from the Israel Science Foundation.

[1] A. Caspi, O. Yeger, I. Grosheva, A.D. Bershadsky, and M. Elbaum, Biophys. J. **85**, 1990 (2001).
[2] R. Granek and S. Pierrat, Phys. Rev. Lett. **83**, 872 (1999).
[3] A. Caspi, R. Granek, and M. Elbaum, Phys. Rev. Lett. **85**, 5655 (2000).
[4] G. Zumofen, J. Klafter, and A. Blumen, Phys. Rev. A **42**, 4601 (1990).
[5] A. Ajdari, Europhys. Lett. **31**, 69 (1995).
[6] X.L. Wu and A. Libchaber, Phys. Rev. Lett. **84**, 3017 (2000).
[7] A. Caspi, M. Elbaum, R. Granek, A. Lachish, and D. Zbaida, Phys. Rev. Lett. **80**, 1106 (1998).
[8] E. Nogales, M. Whittaker, R. A. Milligan, and K. H. Downing, Cell **96**, 79 (1999).
[9] D.K. Fygenson, E. Braun, and A. Libchaber, Phys. Rev. E **50**,

1579 (1994).
[10] L.G. Bergen and G.G. Borisy, J. Cell Biol. **84**, 141 (1980).
[11] R.A. Walker, E.T. O'Brien, N.K. Pryer, M.F. Soboeiro, W.A. Voter, H.P. Erickson, and E.D. Salmon, J. Cell Biol. **107**, 1437 (1988).
[12] S.C. Kuo and M.P. Sheetz, Science **260**, 232 (1993).
[13] J.E. Molloy, J.E. Burns, J. Kendrick-Jones, R.T. Tregear, and D.C. White, Nature (London) **378**, 209 (1995).
[14] K. Svoboda and S.M. Block, Cell **77**, 773 (1994).
[15] H. Kojima, E. Muto, H. Higuchi, and T. Yanagida, Biophys. J. **73**, 2012 (1997).
[16] R.A. Harris and J.E. Hearst, J. Chem. Phys. **44**, 2595 (1966).
[17] S.R. Aragon S and R. Pecora, Macromolecules **18**, 1868 (1985).
[18] J. Wilhelm and E. Frey, Phys. Rev. Lett. **77**, 2581 (1996).
[19] F. Gittes, B. Mickey, J. Nettleton, and J. Howard, J. Cell Biol. **120**, 923 (1993).
[20] P. Venier, A.C. Maggs, M.F. Carlier, and D. Pantaloni, J. Biol. Chem. **269**, 13 353 (1994).
[21] H. Felgner, R. Frank, and M. Schliwa, J. Cell. Sci. **109**, 509 (1996).
[22] M. Elbaum, D.K. Fygenson, and A. Libchaber, Phys. Rev. Lett. **76**, 4078 (1996).
[23] H. Hagashima and S. Asakura, J. Mol. Biol. **136**, 169 (1980).
[24] A. Ott, M. Magnasco, A. Simon, and A. Libchaber, Phys. Rev. E **48**, R1642 (1993).
[25] D. Riveline, C.H. Wiggins, R.E. Goldstein, and A. Ott, Phys. Rev. E **56**, R1330 (1997).
[26] R. Granek, J. Phys. II **7**, 1761 (1997).
[27] A. Caspi, R. Granek, and M. Elbaum, in *Dynamics in Small Confining Systems V*, edited by J. M. Drake, J. Klafter, P. Levitz, R. M. Overney, and M. Urbakh, MRS Symposia Proceedings No. 651 (Materials Research Society, Pittsburgh, 2001), p. T1.2.
[28] K. L. Carraway and C. A. C. Carraway, *The Cytoskeleton* (Oxford University Press, NY, 1992).
[29] T. Gisler and D.A. Weitz, Curr. Opin. Colloid Interface Sci. **3**, 586 (1998).
[30] F. Amblard, A.C. Maggs, B. Yurke, A.N. Pargellis, and S. Leibler, Phys. Rev. Lett. **77**, 4470 (1996).
[31] J. Apgar, Y. Tseng, E. Fedorov, M.B. Herwig, S.C. Almo, and D. Wirtz, Biophys. J. **79**, 1095 (2000).
[32] J.C. Crocker, M.T. Valentine, E.R. Weeks, T. Gisler, P.D. Kaplan, A.G. Yodh, and D.A. Weitz, Phys. Rev. Lett. **85**, 888 (2000).
[33] F. Gittes and F.C. MacKintosh, Phys. Rev. E **58**, R1241 (1998).
[34] E. Farge and A.C. Maggs, Macromolecules **26**, 5041 (1993).
[35] F. Gittes, B. Schnurr, P.D. Olmsted, F.C. MacKintosh, and C.F. Schimdt, Phys. Rev. Lett. **79**, 3286 (1997).
[36] A. Palmer, T.G. Mason, J. Xu, S.C. Kuo, and D. Wirtz, Biophys. J. **76**, 1063 (1999).
[37] T. Gisler and D.A. Weitz, Phys. Rev. Lett. **82**, 1606 (1999).
[38] E. Barkai and J. Klafter, Phys. Rev. Lett. **81**, 1134 (1998).
[39] K. Luby-Phelps, D.L. Taylor, and F. Lanni, J. Cell Biol. **102**, 2015 (1986).
[40] M. Goulian and S.M. Simon, Biophys. J. **79**, 2188 (2000).
[41] M. Wachsmuth, W. Waldeck, and J. Langowski, J. Mol. Biol. **298**, 677 (2000).
[42] A.R. Bauch, W. Moller, and E. Sackmann, Biophys. J. **76**, 573 (1999).
[43] W. Feneberg, M. Westphal, and E. Sackmann, Eur. Biophys. J. **30**, 284 (2001).
[44] W. Moller, I. Nemoto, T. Matsuzaki, T. Hofer, and J. Heyder, Biophys. J. **79**, 720 (2000).
[45] T.G. Mason, K. Ganesan, J.H. van Zanten, D. Wirtz, and S.C. Kuo, Phys. Rev. Lett. **79**, 3282 (1997).
[46] S. Yamada, D. Wirtz, and S.C. Kuo, Biophys. J. **78**, 1736 (2000).
[47] R.D. Vale, B.J. Schnapp, T.D. Reese, and M.P. Sheetz, Cell **40**, 449 (1985).
[48] G.J. Todaro, H. Green, and M.R. Swift, Science **153**, 1252 (1966).
[49] L.A. Lyass, A.D. Bershadsky, V.I. Gelfand, A.S. Serpinskaya, A.A. Stavrovskaya, J.M. Vasiliev, and I.M. Gelfand, Proc. Natl. Acad. Sci. U.S.A. **81**, 3098 (1984).
[50] S.C. Kuo and J.L. McGrath, Nature (London) **407**, 1026 (2000).
[51] H. D. Brunk, *An Introduction to Mathematical Statistics* (Ginn, Boston, 1960), p. 132.
[52] H. Qian, M.P. Sheetz, and E.L. Elson, Biophys. J. **60**, 910 (1991).
[53] R. Kubo, M. Toda, and N. Hashitsume, *Statistical Mechanics II*, 2nd ed. (Springer, Berlin, 1991, 2nd ed.), p. 31.
[54] T.G. Mason and D.A. Weitz, Phys. Rev. Lett. **74**, 1250 (1995).
[55] K.G. Wang and M. Tokuyama, Physica A **265**, 341 (1999).
[56] H. Scher and M. Lax, Phys. Rev. B **7**, 4491 (1973).
[57] Y. Liu, G.J. Sonek, M.W. Berns, K. Konig, and B.J. Tromberg, Opt. Lett. **20**, 2246 (1995).
[58] E.L. Florin, J.K.H. Horber, and E.H.K. Stelzer, Appl. Phys. Lett. **69**, 446 (1996).
[59] Carboxylated silica beads 0.3 μm diameter, from Bangs labs (3 μl, 10% solids) were gently mixed with tris (hydroxymethyl) aminomethane solution (50 mg/0.5 ml) for 2 h at room temperature. The beads were washed three times with 0.5 ml distilled water and suspended in 1 ml microtubule polymerization buffer.